V. Shlyannikov et alii, Frattura ed Integrità Strutturale, 35 (2016) 114-124; DOI: 10.3221/IGF-ESIS.35.14

Focussed on Crack Paths

Surface crack growth subject to bending and biaxial tension-compression

V. Shlyannikov, A. Tumanov, A. Zakharov
Kazan Scientific Center of Russian Academy of Sciences, Russia
shlyannikov@mail.ru, tymanoff@rambler.ru, alex.zakharov88@mail.ru

A. Gerasimenko
Saint-Petersburg University of Mines, Russia
anastasiya.geras@mail.ru

ABSTRACT. Fatigue surface crack growth and the in-plane and out-of-plane constraint effects are studied through experiments and computations for aluminium alloy D16T. Subjects for studies are cruciform specimens under different biaxial loading and bending central notched specimens with external semi-elliptical surface crack. Both the optical microscope measurements and the crack opening displacement (COD) method are used to monitor and calculate both crack depth and crack length during the tests. The variation of crack growth rate and surface crack paths behaviour is studied under cyclic pure bending and biaxial tension-compression fatigue loading. This work is centered on the relations between crack size on the free surface of specimen considered configurations, COD and aspect ratio under different fatigue loading conditions. For the experimental surface crack paths in tested specimens the T-stress, the local triaxiality parameter h, the out-of-plane T_Z factor and the governing parameter for the 3D-fields of the stresses and strains at the crack tip in the form of I_n-integral were calculated as a function of aspect ratio by finite element analysis to characterization of the constraint effects along semi-elliptical crack front. The plastic stress intensity factor approach is applied to the fatigue crack growth on the free surface of the tested bending and cruciform specimens as well as the deepest point of the semi-elliptical surface crack front. As result fatigue surface crack paths or crack front positions as a function of accumulated number of cycle of loading are obtained.

KEYWORDS. Surface crack; Biaxial loading; Bending; Crack growth.

INTRODUCTION

In order to provide operation in a safe condition, it is necessary to perform fracture mechanics assessment of a structural component under cyclic loading. The fatigue growth analysis of surface cracks is one of the most important elements for structural integrity prediction of the flat metallic components in the presence of initial and accumulated operation damages. In most cases, part-through flaws appear on the free surface of the structures and defects

are approximately considered as semi-elliptical cracks. Biaxial loading conditions including tension/compression and bending are typical for the metallic components of engineering structures (turbine disk, aeroplane fuselage skin, pressure vessels and so on). The problem of residual fatigue life prediction of such type of structural elements is complex and the closed solution is often not available because surface flaws are three-dimensional in nature. The fatigue failure of structural elements subjected to biaxial stress system maybe develops from surface flaws, and only several analyses have been carried out to determine the stress intensity factors along the front of an edge defects and crack growth rate study on this base [1-4]. An actual surface crack may usually be replaced by an equivalent circular arc or elliptical-arc edge flaw. The elastic stress intensity factors have been published for part-circular, part-elliptical, or straight fronted through-thickness cracks in a cruciform and bending specimens.

In this paper, firstly experimental results of fatigue crack growth for a crack starting from a semi-elliptical notch in an cruciform specimens under biaxial loading and bending plate are given. The influence of different loading conditions on fatigue life of cruciform specimens and bending plate is discussed. The relations of crack opening displacement and crack length on the free surface of specimens are obtained and it is shown that the growth of the crack fronts is dependent on the initial notch form. Using the aforementioned relations, the crack front shape and crack growth rate in the depth direction can be predicted. The simulations for the crack path assessment are based on the constraint parameters behaviour. The computational 3D fracture analyses deliver a governing parameter of elastic-plastic stress field distributions along the crack front. On this base crack growth interpretation is performed using the traditional elastic and new plastic stress intensity factors [5-7]. Different crack growth rate is observed in the direction of the deepest point of the crack front with respect to the free surface of the bending specimen.

SPECIMENS AND MATERIAL PROPERTIES

The test material is aluminum alloy D16T which main mechanical properties are listed in Tab. 1 where E is the Young's modulus, σ_b is the nominal ultimate tensile strength, σ_0 is the monotonic tensile yield strength, σ_u is the true ultimate tensile strength, δ is the elongation, ψ is the reduction of area, n is the strain hardening exponent and α is the strain hardening coefficient.

Aluminum alloy	$\sigma_{0.2}$ MPa	σ_b MPa	δ %	ψ %	σ_u MPa	E GPa	n	α
D16T	439	590	9	9	645	75.922	5.88	1.50
	438	598	12	13	686	77.191	5.85	1.58

Table 1: Main mechanical properties of aluminum alloys.

The cruciform specimen (CS) geometry and bending plate (BP) configuration are shown in Fig. 1. The thickness of both specimens is equal to 10 mm. Using linear cutting machine surface edge cracks were cut with initial flaw depths b_0 3.0 mm for both a circular arc and elliptical-arc initial edge notch. The geometric parameters of the specimens and initial notch are shown in Fig. 1. In this figure, the crack front approximated by an elliptical curve with major axis $2c$ and minor axis 2a. The crack length on the free surface of specimen c is obtained by measuring the distance between the advancing crack break through point and the notch break through point. The crack opening displacement is measured on the free specimen flat surface, in the central plane of symmetry as shown in Fig. 2.

The CS fatigue crack growth tests have been performed with servohydraulic biaxial test equipment at a frequency of 5 Hz at a stress ratio R=0.1. The equipment has four independent loading arms with load actuators, which exert up to 50 kN on the both axes. Tensile or compressive loads are applied to each pair of arms of the cruciform specimens (Fig. 1), developing a biaxial stress field in the working section. The loads are controlled such that the specified forces are produced on opposing arms of the CS according to the given load biaxiality. For pure mode I at crack angle equal α = 90°, four biaxial load ratios for CS, λ equal to +1.0, +0.5, 0.0 (uniaxial), and -1.0. Bending tests were carried out on servo-hydraulic test system BISS-nano with maximal capacity 25 kN at a frequency of 7 Hz at a stress ratio R=0.1. The crack length on the specimen lateral surface were monitored using the optical instrumental zoom microscope whereas, to fix the

crack opening displacement of specimen at the gauge length, a pulley arrangement with an externally axial encoder is introduced (Fig. 2). All tests are carried out with sinusoidal loading form with load control.

Two different stress ratio R_f values (0.1 and 0.5) were applied several times to the specimens in order to highlight the crack front geometry during propagation: during each test, beach marks were produced on each specimen by increasing the applied stress ratio from 0.1 to 0.5 at constant value of maximum cyclic nominal stress, when the surface crack length was approximately increased to $a \cong 0.1$mm. The typical beach marks on the post mortem cross section of different specimens are shown in Figs. 2 and 3 for biaxial tension and bending, respectively. From the crack front shape obtained in

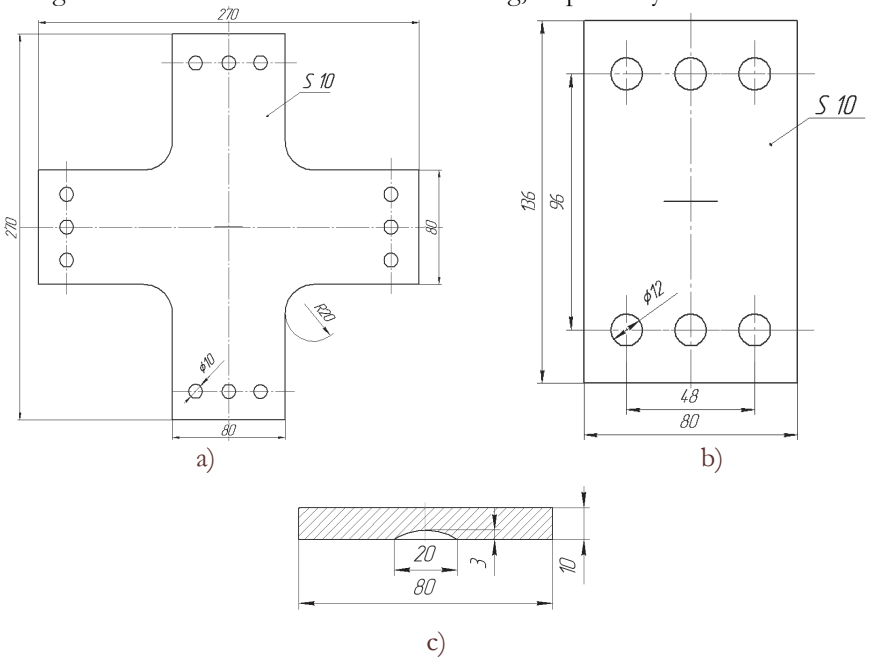

Figure 1: Details of the (a) cruciform specimen and (b) plate geometry and (c) initial notches.

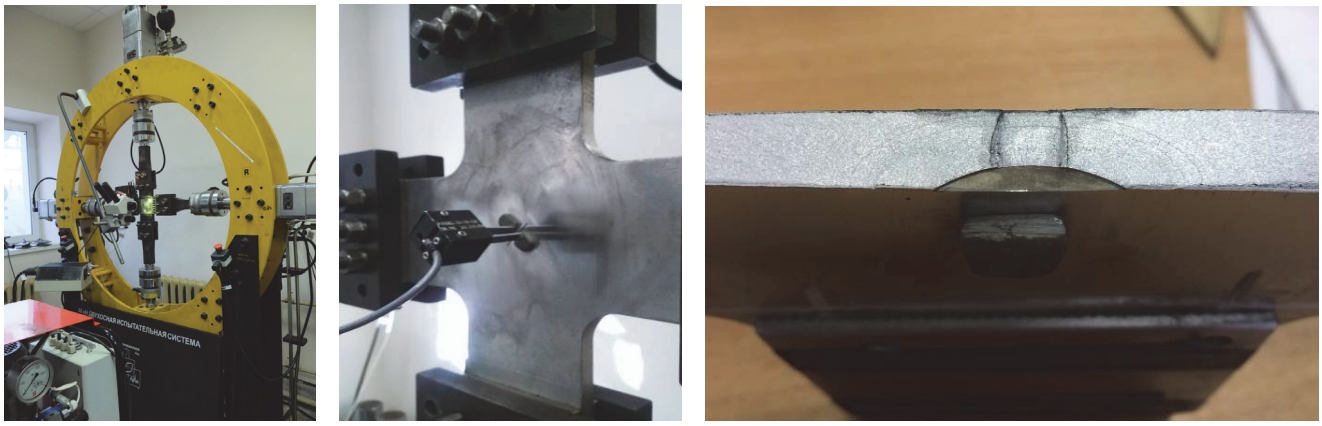

Figure 2: Test equipment for measuring COD and crack path under biaxial loading.

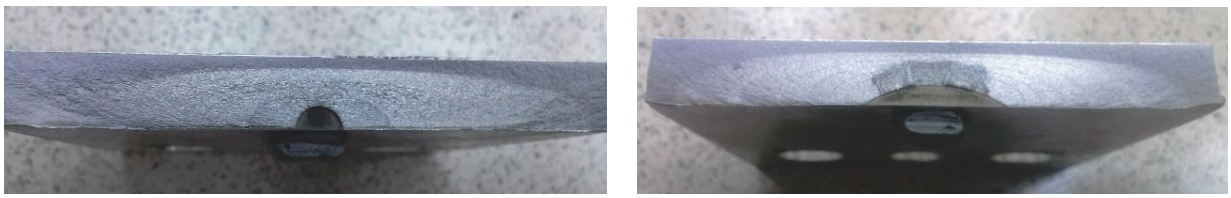

a) b)

Figure 3: Surface crack paths under bending for initial aspect ratio (a) $(a/c)_0$=1.0 and (b) $(a/c)_0$=0.36.

this way, the relations between the relative crack depth a/t and the aspect ratio a/c can be measured using a comparison microscope. In addition, based on periodically measured increments of surface crack length Δc, the curve of surface crack propagation versus cycle numbers dc/dN can be obtained. Afterwards, utilizing the relation of crack depth versus surface crack length, it is possible to obtain the crack growth rates da/dN in the depth direction. Another interesting result pointed out in the present study is the aspect ratio increasing under biaxial loading as a function of crack depth a/t (Fig.4,a) whereas the aspect ratio decreasing under bending loading (Fig.4,b).

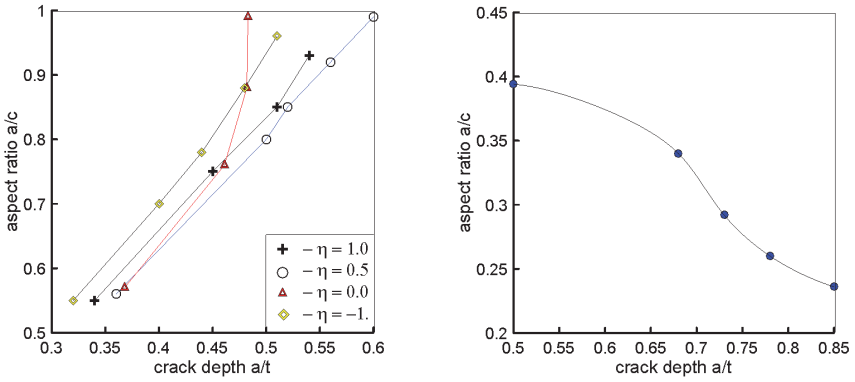

a) b)

Figure 4: Aspect ratio versus crack depth under (a) different biaxial loading and (b) bending.

NUMERICAL RESULTS

From Figs. 2 and 3 can be seen that the length of the arc of semi-elliptical crack front depends on the loading conditions of the CS and BP specimens. Moreover, the crack propagation process in CS samples can be divided into two stages. During the first stage a semi-elliptical crack is a part-through-thickness. On the second stage semi-elliptical crack completely crosses the wall and becomes a through-thickness. To compare the parameter distributions along the semi-elliptical crack front is convenient to introduce the dimensionless coordinates in the following form $\bar{\varphi} = 2\varphi/\pi$. In the following representation of numerical results, we will use variable $\bar{\varphi}$ changing in the range from 0 to 1.

Constraint parameters

Characterization of the constraint effects in the present study was performed using the non-singular T-stresses, the local triaxiality parameter h and the T_Z-factor of the stress-state in a 3D cracked body to illustrate the features of the behavior of surface cracks in the CS and BP specimens.

T-stress

Using the crack flank nodal displacements technique, the T-stress distributions in various specimen geometries were determined from numerical calculations. To this end, the commercial finite element code, ANSYS [8], was used to calculate the stress distributions ahead of the crack tips. In this part of the FEA calculations, the material is assumed to be linear elastic and characterized by E=76.5 GPa and ν=0.3.

T_z-factor

The T_Z factor [9] has been recognized to present a measure of the out-of-plane constraint and can be expressed as the ratio of the normal elastic-plastic stress components

$$T_z = \frac{\sigma_{zz}}{\sigma_{xx} + \sigma_{yy}} \tag{1}$$

where σ_{zz} is the out-of-plane stress, and σ_{xx} and σ_{yy} are the in-plane stresses. The variation of this parameter is important to characterize the thickness effect on the crack front stress distribution and the changes of the plastic zone size.

Stress triaxiality

As a secondary fracture parameter, a local parameter of the crack-tip constraint was proposed by the authors [10] because the validity of some of the above-mentioned concepts depends on the chosen reference field. This stress triaxiality parameter is described as follows:

$$h(r,\theta,z)=\sigma_{kk}\Big/\left(3\sqrt{\frac{3}{2}s_{ij}s_{ij}}\right) \tag{2}$$

where σ_{kk} and s_{ij} are the hydrostatic and deviatoric stresses, respectively. Being a function of both the first invariant of the stress tensor and the second invariant of the stress deviator, the stress triaxiality parameter is a local measure of the in-plane and out-of-plane constraint that is independent of any reference field.

Plastic stress intensity factor

Here, our primary interests are to obtain an accurate description for the distribution along the crack front of the governing parameter for the elastic-plastic solution in the form of an I_n-integral and to determine the accuracy that this type of calculation, which will later be used for the general 3D problem, provides for the plastic stress intensity factor (SIF). The method developed here for combining the knowledge of the dominant singular solution with the finite element technique to obtain accurate solutions in the neighborhood of a crack tip is also applicable to the treatment of problems involving cracks in finite bodies. The plastic stress intensity factor K_P in pure Mode I can be expressed directly in terms of the corresponding elastic stress intensity factor using Rice's *J*-integral. That is

$$\overline{K}_P=\left[\frac{\left(\overline{K}_1^2\right)}{\overline{\alpha}\sigma_0^2 I_n(\theta)}\right]^{1/(n+1)}=\left[\left(\frac{\sigma}{\sigma_0}\right)^2\frac{\pi\lambda}{\overline{\alpha}}\frac{Y_1^2(a/w)}{I_n(\theta)}\right]^{1/(n+1)};\ \overline{K}_1=\sigma\sqrt{\pi\lambda}\cdot Y_1(a/w) \tag{3}$$

where $\overline{K}_1=K_1/\sqrt{w}$ is normalized by a characteristic size of cracked body elastic stress intensity factor and $E'=E$ for plane stress and $E'=E/\left(1-\nu^2\right)$ for plane strain. In the above equations, $\overline{\alpha}$ and n are the hardening parameters, $\lambda=a/w$ is the dimensionless crack length, w is characteristic size of specimen (for our case that is specimen width), σ is the nominal stress, and σ_0 is the yield stress. The numerical constant $I_n(\theta)$ is obtained from the singularity analysis by means of the conjugation solutions for the far and near fields. In the classical first-term singular HRR-solution [11], the numerical parameter I_n is a function of only the material strain hardening exponent n. Shlyannikov and Tumanov [5] reconsidered the HRR-solution for both plane strain and plane stress and supposed that under small-scale yielding, the expression for I_n depends implicitly on the dimensionless crack length and the specimen configuration. In this section, we extend the analysis to the I_n-integral behavior in an infinitely sized cracked body [11] to treat the test specimen's specified geometries. The use of the Hutchinson's theoretical definition for the *In*-factor directly adopted in the numerical finite element analyses leads to [5]

$$I_n^{FEM}\left(\theta,n,\left(\frac{c}{w},\frac{a}{t}\right)\right)=\int_{-\pi}^{\pi}\left\{\begin{array}{l}\dfrac{n}{n+1}\left(\tilde{\sigma}_e^{n+1}\right)^{FEM}\cos\theta-\left[\tilde{\sigma}_{rr}^{FEM}\left(\tilde{u}_\theta^{FEM}-\dfrac{d\tilde{u}_r^{FEM}}{d\theta}\right)-\tilde{\sigma}_{r\theta}^{FEM}\left(\tilde{u}_r^{FEM}+\dfrac{d\tilde{u}_\theta^{FEM}}{d\theta}\right)\right]\sin\theta-\\ -\dfrac{1}{n+1}\left(\tilde{\sigma}_{rr}^{FEM}\tilde{u}_r^{FEM}+\tilde{\sigma}_{r\theta}^{FEM}\tilde{u}_\theta^{FEM}\right)\cos\theta\end{array}\right\}d\theta \tag{4}$$

In this case, the numerical integral of the crack tip field I_n changes not only with the strain hardening exponent n but also with the relative crack length c/w and the relative crack depth a/t. More details to determine the I_n factor for different test specimen configurations are given by Refs. [5-7].

The distributions of the elastic and elastic-plastic constraint parameters along the crack front in the bending specimen under cyclic loading are plotted in Figs. 6 and 7. These distributions correspond to the crack front positions at the accumulated number of loading cycles N_1=0 (initial front), N_2= 28000 (intermediate front), N_3= 38000 (intermediate front), N_4= 44500 (final failure front). The constraint parameter is plotted against the normalized coordinate $\bar{\varphi}$. In this plot $\bar{\varphi}$ = 0.0 is the crack border (the specimen free surface) while $\bar{\varphi}$ = 1.0 is the mid-plane of the specimen thickness. It can be observed that all constraint parameters essentially changed along the crack front from the free surface toward the mid-plane.

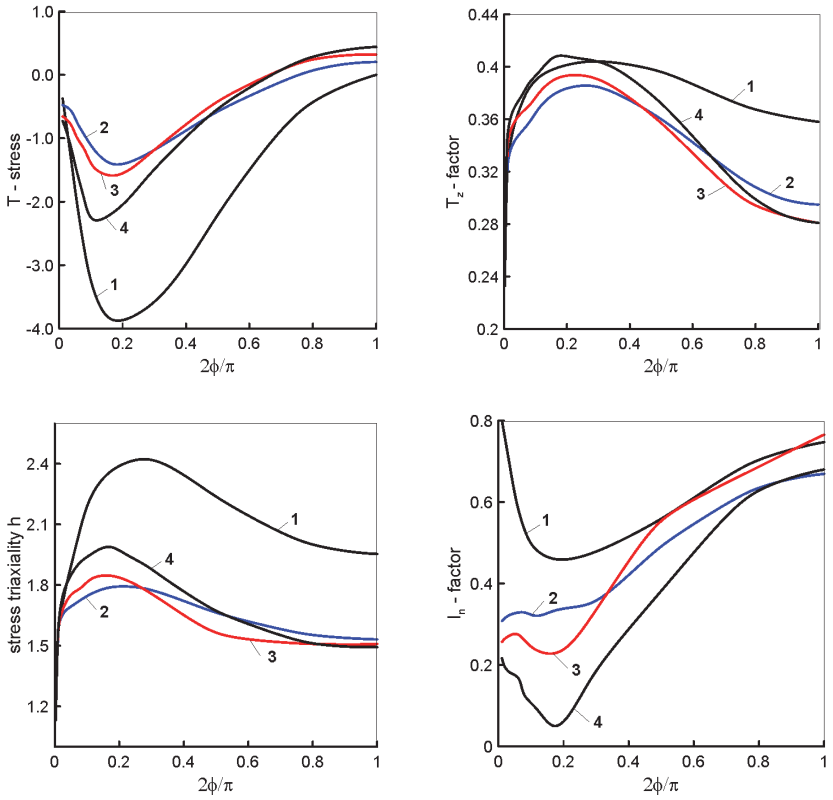

Figure 5: Constraint parameter distributions for bending plate along crack front (1-initial, 2-3-intermediate, 4-final).

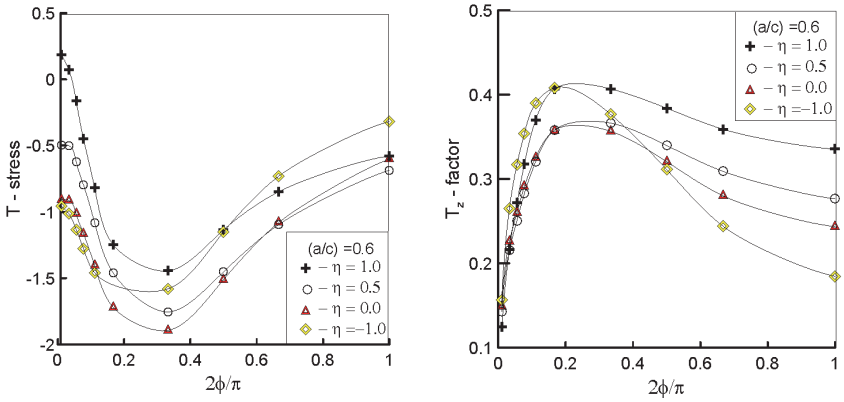

Figure 6: Elastic constraint parameter distributions along crack front under different biaxial loading conditions.

The distribution of the elastic-plastic constraint parameters along the crack front in the direction from the free surface toward the mid-plane is plotted in Figs. 6 and 7 for the cruciform specimens under different biaxial loading conditions. The constraint parameters are plotted against the normalized angular coordinate $\bar{\varphi}$. It can be observed from these figures that all constraint parameters sufficiently changed along the crack front from the free surface toward the mid-plane as a

function of load biaxiality. Fig. 6 represents the distributions of the constraint parameters for the biaxial tension and as well as the combined tension-compression loading for the intermediate crack front position (a/c)=0.6.
The last part of the numerical calculations of the present study is devoted to the determination of the elastic and plastic stress intensity factors in cruciform and bending samples. In Fig.8 shown the distributions of the elastic and plastic SIFs for the same tensile loading conditions along the same crack front in the CS configuration. Fig. 8 gives a clear illustration of the necessity to take into account the load biaxiality in order to the interpretation of the characteristics of the material resistance to crack propagation. The data shown in Fig. 9 the distributions of the elastic and plastic SIFs related to the bending plate in more details for several crack front positions.

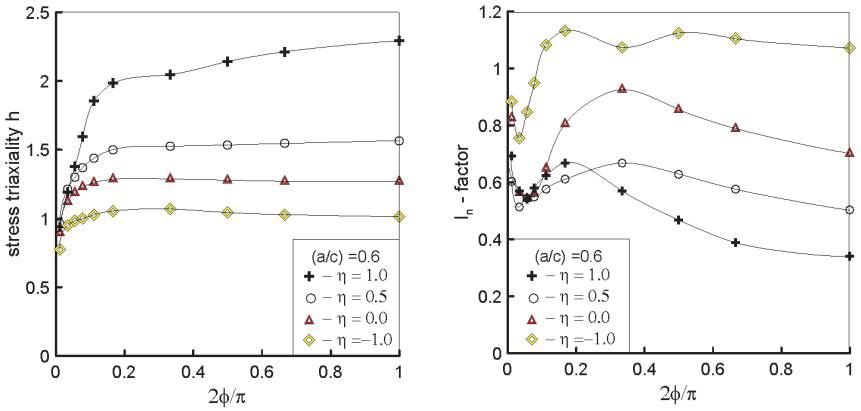

Figure 7: Plastic constraint parameter distributions along crack front under different biaxial loading conditions.

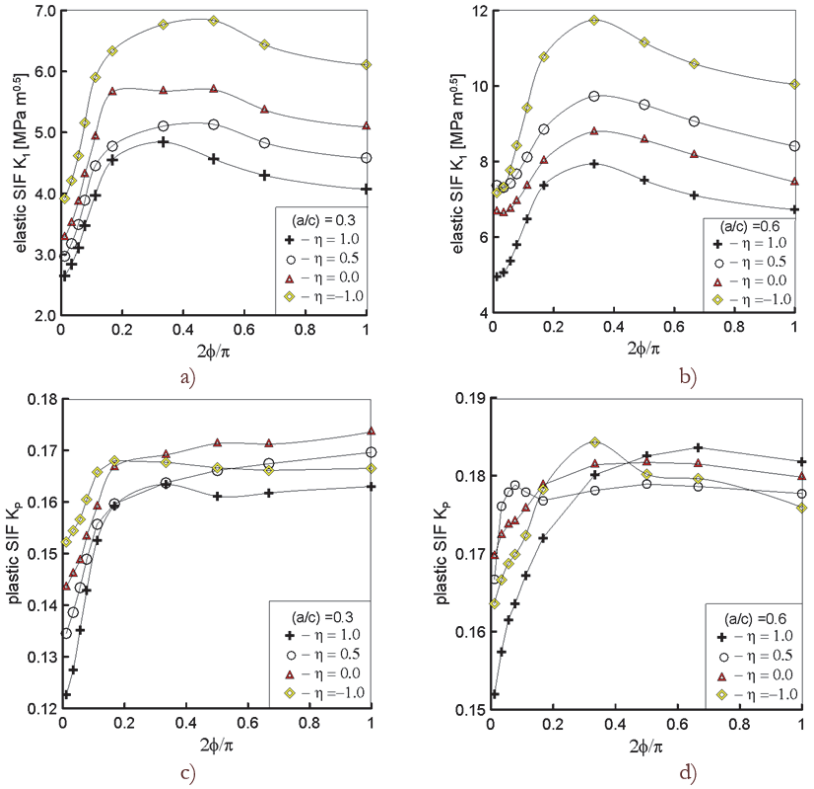

Figure 8: Elastic (a,b) and plastic (c,d) stress intensity factor behavior for different aspect ratio under biaxial loading.

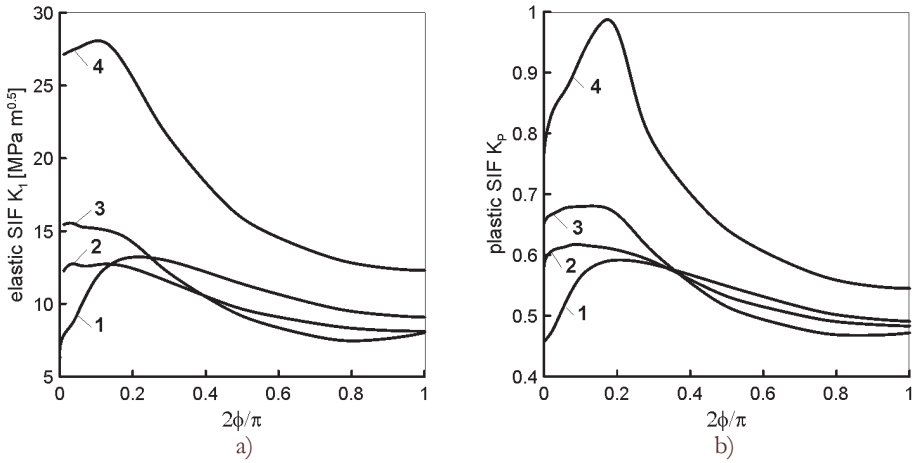

Figure 9: Elastic (a) and (b) plastic stress intensity factor distributions for bending plate along crack front (1-initial, 2-3-intermediate, 4-final).

EXPERIMENTAL RESULTS AND DISCUSSION

The evolution of the crack growth rate of the elliptical-fronted edge cracks during the tests is determined using COD and the microscope. In order to study the crack growth under fatigue tension-compression biaxial loading and bending, several flat specimens of aluminum alloy D16 are tested with an initial notch depth equal to 3 mm. Fig. 10 shows plot of the break through point advances c and of COD against the number of cycles N under different biaxial loading and bending, respectively. As shown in Fig. 10, in-phase cyclic tension-compression leads to different effects on the relationship between crack length on the free surface and crack opening displacement for the cruciform specimens and bending plate for the same main material properties. Nevertheless there is a strong correlation between these two parameters that can be very useful for automation of experimental studies of fatigue and fracture under multiaxial stress state. On the base of this experimental data, polynomial functions can be used to express the COD as a function of the superficial crack length.

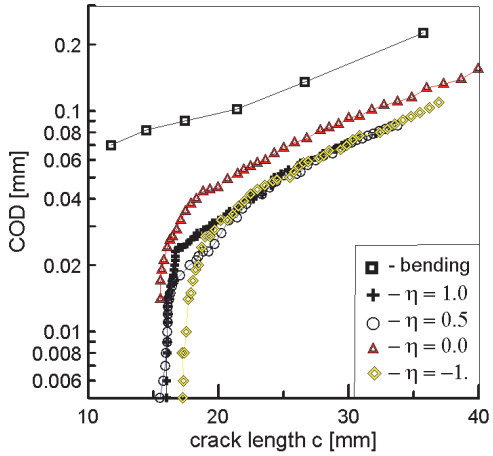

Figure 10: Relationship between COD and crack length on free surface of cruciform specimens and bending plate.

Fig. 11a represents the superficial crack growth rate dc/dN versus COD on the cruciform specimens undergoing pure Mode I tension and compression loading. It is found that the crack growth rate along the external surface direction as a function of COD fit into a single curve with a small scatter band of the experimental results under different loading conditions when $(dc/dN)>10^{-4}$ m/cycle and COD>0.4 mm. Thus, load biaxiality has a significant influence on the initial stage of surface flaw growth. The bending plate (Fig. 11b) has a smaller range of crack growth rates as compared to biaxially loaded CS samples. However, looking at Fig. 3 and Fig. 4b, significant differences in the crack growth rate in the depth direction a and on the free surface c are expected.

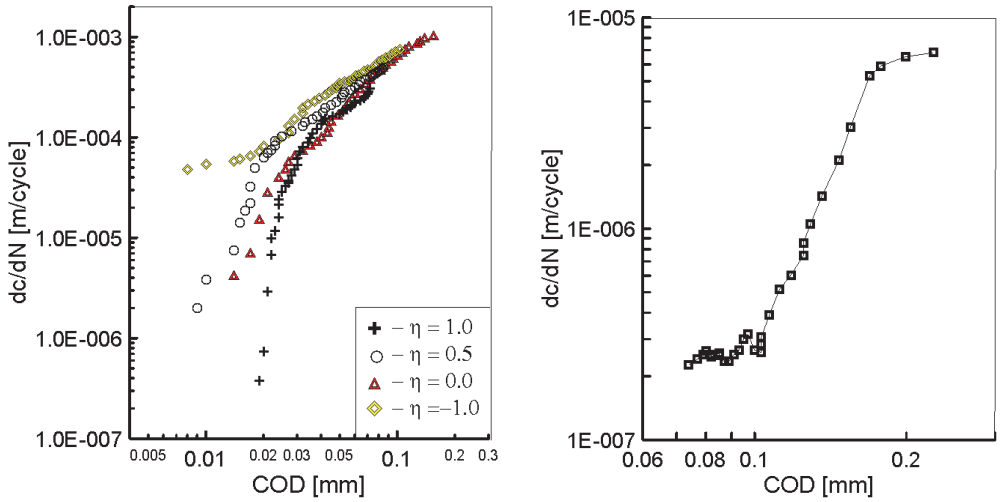

Figure 11: Crack growth rate on free surface of (a) cruciform specimens and (b) bending plate versus COD.

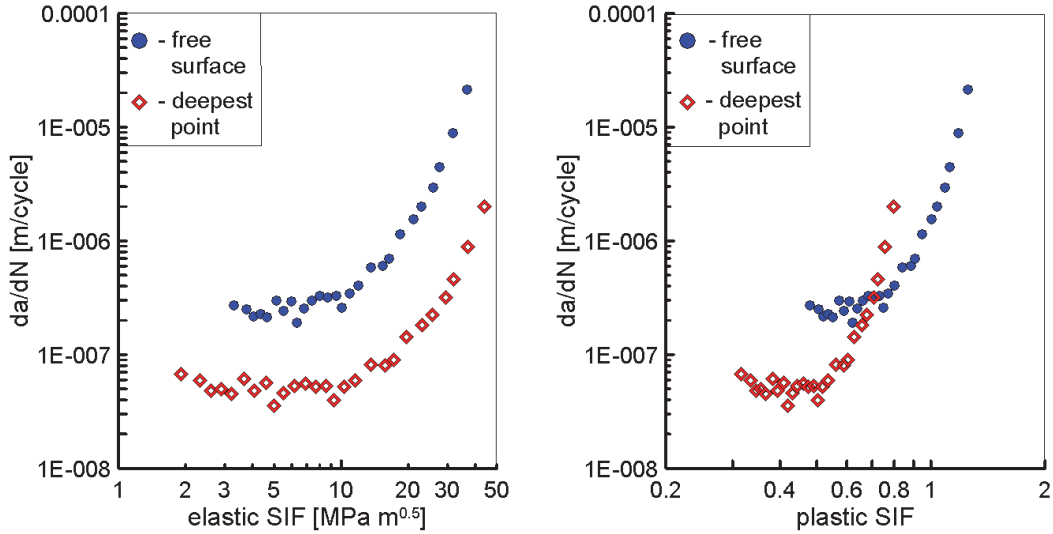

Figure 12: Crack growth rate as a function of (a) elastic and (b) plastic SIFs under bending for different crack front points.

Fig. 12 shows the typical experimental fatigue fracture diagrams in the coordinates of the crack growth rate versus the values of the stress intensity factors for the plate tested under bending loading. The left picture in Fig. 12 depicts the behavior of the da/dN and dc/dN as a function of the elastic SIF K_I, whereas the right picture in Fig. 12 gives us the crack growth rate depending on of the dimensionless plastic stress intensity factor K_P. To determine the experimental values of the elastic and plastic SIFs for two main points of the crack front, namely, the free surface a and mid-plane section c, was used the distributions represented in Fig. 9. Looking at Fig.12 it should be noted that a significant reduction of the crack growth rates is observed in the direction of the deepest point of the crack front with respect to the crack front intersection with the free surface of the bending specimens in terms of the elastic and plastic SIFs.

In contrast to the elastic SIF K_I, the plastic SIF K_P shows very useful effect of the sensitivity to the plastic properties of the tested materials. It can be seen from Fig. 12 that the plastic SIF gradually increases by increasing the crack length and crack depth at fixed elastic properties of the aluminum alloy characterized by E=76 GPa and ν=0.3. The data presented very obvious advantages of using the plastic stress intensity factors to characterize the material's resistance to cyclic crack growth. This conclusion is confirmed by the relative position of crack growth curves in Fig.12 for the tested aluminum alloy D16 in the terms of the elastic and plastic SIFs.

CONCLUSIONS

Fatigue crack growth for a semi-elliptical crack with two different initial notch form in cruciform specimens and bending plate of D16 aluminum alloy is studied. Experiments and calculations made under biaxial cyclic tension-compression and bending are described. All the experimental and numerical results are shown:

- for the same specimen configuration and different the crack front position as a function of cyclic tension-compression and bending loading, the following constraint parameters were analyzed, namely, the non-singular T -stress, T_z -factor and the stress triaxiality parameter h in the 3D series of elastic-plastic computations;
- the governing parameter of the elastic-plastic stress fields I_n-factor distributions along various crack fronts was also determined from numerical calculations, this governing parameter is used as the foundation of the elastic-plastic stress intensity factor;
- under cyclic bending, it can be seen that the crack propagation paths differ with diverse initial flaw forms, but under biaxial loading converge to the same configuration when the crack depth ratio is larger than about 0.5;
- it is found that there is relationship between the crack growth rate on the free surface of specimen and COD for both tested cruciform specimens and bending plate;
- a significant reduction of the crack growth rates is observed in the direction of the deepest point of the crack front with respect to the crack front intersection with the free surface of the bending plate;
- the experimental and numerical results of the present study background provide an opportunity to explore the suggestion that crack growth rate may be represented by the plastic stress intensity factor, rather than the magnitude of the elastic SIFs alone;
- it is stated that the elastic-plastic stress intensity factor, which is sensitive to the constraint effects and elastic-plastic material properties, is attractive as the self-dependent unified parameter for characterization of the material fracture resistance properties.

ACKNOWLEDGMENT

The authors gratefully acknowledge the financial support of the Russian Scientific Foundation under the Project 14-19-01716.

REFERENCES

[1] Newman, J.C., Raju, I.S., An empirical stress-intensity factor equation for the surface crack, Eng. Fract. Mech., 15 (1-2) (1981) 185-192.
[2] Carpinteri, A., Brighenti, R., Part-through cracks in round bars under cyclic combined axial and bending loading, Int. J. Fatigue, 18 (1) (1996) 33-39.
[3] Shlyannikov, V.N., Tumanov, A.V., An inclined surface crack subject to biaxial loading, Int. J. Solids Struct., 48 (2011) 1778-1790.
[4] Shlyannikov, V.N., Kislova S.Yu., Tumanov, A.V., Inclined semi-elliptical crack for predicting crack growth direction based on apparent stress intensity factors, Theoret. Appl. Fract. Mech., 53 (2010) 185-193.
[5] Shlyannikov, V.N., Tumanov, A.V., Characterization of crack tip stress fields in test specimens using mode mixity parameters, Int. J. Fract., 185 (2014) 49-76.
[6] Shlyannikov, V.N., Zakharov, A.P., Multiaxial crack growth rate under variable T-stress, Eng. Fract. Mech., 123 (2014) 86–99.
[7] Shlyannikov, V.N., Tumanov, A.V., Zakharov, A.P., The mixed mode crack growth rate in cruciform specimens subject to biaxial loading, Theoret. Appl. Fract. Mech., 73 (2014) 68-81.
[8] ANSYS Mechanical APDL Theory Reference Release 14.5// ANSYS, Inc. Southpointe, 275 Technology Drive, CanonBurg, PA 2012.
[9] Guo, W.L., Elasto-plastic three dimensional crack border field-I, Eng. Fract. Mech., 46 (1993) 93-104.

[10] Henry, B.S., Luxmoore, A.R., The stress triaxiality constraint and the Q-value as ductile fracture parameter, Eng. Fract. Mech., 55 (1997) 375-390.
[11] Hutchinson, J.W., Singular behaviour at the end of a tensile crack in a hardening material, Journ. Mech. Phys. Solids, 16 (1968) 13-31.